Journal of Alloys and Compounds 513 (2012) 425–429

Contents lists available at SciVerse ScienceDirect

Journal of Alloys and Compounds

journal homepage: www.elsevier.com/locate/jallcom

Synthesis and characterization of magnetite powders obtained by the solvothermal method: Influence of the Fe^{3+} concentration

Malick Jean*, Virginie Nachbaur, Jean-Marie Le Breton

Groupe de Physique des Matériaux, UMR CNRS 6634, Université de Rouen, 76801 St Etienne du Rouvray, France

ARTICLE INFO

Article history:
Received 21 October 2010
Received in revised form 20 October 2011
Accepted 21 October 2011
Available online 7 November 2011

Keywords:
Magnetite
XRD
Mössbauer
Nanostructures
Oxides

ABSTRACT

Nonstoichiometric magnetite particles are prepared via a polyol process using ethylene glycol as a solvent and reducing agent. The powders are investigated by XRD, SEM, Mössbauer spectroscopy and SQUID magnetometry. The influence of the initial concentration of Fe^{3+} ions on both particle size and morphology is investigated. For 0.1 and 0.3 mol L^{-1} concentrations, the particles are spherical (with a diameter between 100 and 350 nm) and composed of nanocrystallites (sized between 20 and 43 nm). For 0.8 mol L^{-1} concentration, the particles are quasi-monocrystalline compact spheres with a diameter between 100 and 250 nm. XRD analysis and Mössbauer spectroscopy show that the smaller the crystallites are, the more oxidized the samples are. The saturation magnetization decreases when the particle size decreases and when the oxidation degree increases.

1. Introduction

Magnetite (Fe_3O_4) powders have excellent magnetic properties and are used for many applications. For example Fe_3O_4 particles have attracted growing interest in water treatment and environmental remediation [1,2]. Furthermore Fe_3O_4 has a good bio-compatibility and a low toxicity so magnetite nanoparticles have a considerable potential for use in biomedical applications such as targeted drug delivery, contrast agent and cancer therapy [3–5]. Finally, Fe_3O_4 can be used in ferrofluid technology [6] or as an electrode in lithium ion batteries [7]. The physical and chemical properties of magnetite strongly depend on the synthesis route. To date, different synthesis processes have been reported, such as the mechanochemical process [8], chemical precipitation [9], autocombustion [10], thermal decomposition [11] or the polyol process [12]. The polyol process is a chemical route which relates to the use of polyols (ethylene glycol, diethylene glycol, etc.) as solvent and reducing agent. This synthesis route is easy to operate as it does not require protective gas to avoid oxidation of Fe^{2+}, thus being a single-step process to obtain magnetite particles.

Fe_3O_4 magnetite has a spinel type structure (i.e., a structure similar to that of the $MgAl_2O_4$ mineral spinel). The AB_2O_4 spinel structure type can be described by a cubic close packing of O^{2-} ions in which A and B cations occupy one in eight tetrahedral sites (A site) and one in two octahedral sites (B site). Magnetite is usually an inverse spinel: the tetrahedral sites are occupied by Fe^{3+} ions and the octahedral sites are randomly occupied by Fe^{2+} and Fe^{3+} ions with the same proportions. Its structural formula can therefore be written as $(Fe^{3+})[Fe^{2+}Fe^{3+}]O_4$ where the different brackets denote the different sites [13,14]. Fe^{2+} ions are easily oxidized and it is possible to prepare nonstoichiometric magnetite with a deficit of iron. These compounds can be described by the formula $(Fe^{3+})_A[Fe^{2+}{}_{(1-x)}Fe^{3+}{}_{(1+2x)}\square_x]_BO_4$ $(0<x<0{,}33)$ where $\square$ denotes vacancies.

In this paper, the polyol synthesis is used to prepare magnetite and the influence of the starting reagent concentration on the morphology and on the magnetic properties is presented.

2. Experimental

2.1. Synthesis

The synthesis is performed using the solvothermal method in ethylene glycol. The typical preparation procedure is as follows: after dissolving $FeCl_3$, $6H_2O$ (Acros 99%) in ethylene glycol (Merck 99%), CH_3CO_2Na (Prolabo 98%) is added and the agitation is maintained for 30 min. This solution is then poured into a Teflon lined bomb (Parr Instruments). The reactor is closed, heated at 200 °C and the temperature is maintained for 21 h. After cooling the reactor, the dark precipitate is separated from the mother liquor by centrifugation, washed with deionized water and ethanol and dried at 60 °C for 24 h.

For all the experiments the ratio between acetate ions and Fe^{3+} ions is equal to 3 and the iron concentration in the starting solution is variable. In the following text, the samples are denoted Fe0.1, Fe0.3 and Fe0.8 and correspond to iron concentrations of 0.13, 0.27 and 0.78 mol L^{-1} respectively.

* Corresponding author. Tel.: +33 02 32 95 50 64; fax: +33 02 32 95 50 72.
E-mail address: malick.jean@univ-rouen.fr (M. Jean).

0925-8388/$ – see front matter © 2011 Elsevier B.V. All rights reserved.
doi:10.1016/j.jallcom.2011.10.064

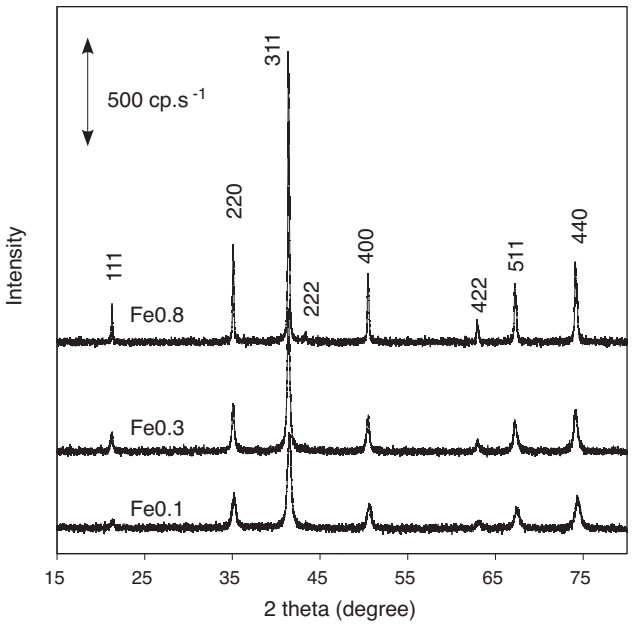

Fig. 1. XRD patterns of the Fe0.1, Fe0.3 and Fe0.8 powders.

Table 1
Lattice parameter and crystallite size for Fe0.1, Fe0.3 and Fe0.8 samples deduced from XRD analysis.

Sample	Lattice parameter (Å)	Crystallite size (nm)
Fe0.1	8.377 ± 0.003	20 ± 2
Fe0.3	8.391 ± 0.003	43 ± 4
Fe0.8	8.396 ± 0.003	121 ± 10
Fe_3O_4 (JCPDS file no. 19-0629)	8.39600	–
γ-Fe_2O_3 (JCPDS file no. 39-1346)	8.35150	–

2.2. Characterization

X-ray powder diffraction (XRD) analysis is performed on a D8 Diffractometer (Bruker AXS), using Co Kα radiations ($\lambda_{K\alpha1} = 0.178897$ nm and $\lambda_{K\alpha2} = 0.179285$ nm). The intensity was measured with a 2θ step of 0.01°. Each diffraction peak is fitted with a pseudo-Voigt function using the Winplotr program (http://www.inpg.fr/LMGP) in order to accurately determine its position and width. The lattice parameter is then calculated with the Checkcell program (http://www.inpg.fr/LMGP) and the crystallite size is obtained using the XRD profile analysis described by Langford [15]. Powders are observed by Scanning Electron Microscopy (Zeiss 1530). The mean sizes of the particles and the crystallites were determined by measuring more than 50 particles or crystallites, and in each case, the dispersion was determined by calculating the standard deviation. Mössbauer spectra in transmission geometry were collected at room temperature with a ^{57}Co γ-ray source in a Rh matrix. The sample thickness is adjusted so that the Fe content is ~10 mg/cm^2 and velocity and isomer shift calibrations are performed using Fe foil as a standard. Hyperfine parameters are denoted: δ for isomer shift (mm s^{-1}), Δ for quadrupolar splitting (mm s^{-1}), ε for quadrupolar shift (mm s^{-1}) and B for magnetic hyperfine field (T). The magnetic measurements (hysteresis loops) are performed at room temperature and at 5 K using a SQUID magnetometer (Quantum Design MPMSXL).

3. Results and discussion

3.1. Structural properties

The X-ray diffraction patterns of the as-prepared powders with different concentrations of iron ions are shown in Fig. 1. In each case, all lines can be indexed using the JCPDS file no. 19-0629 corresponding to magnetite. No other peak is observed, indicating that the samples are single spinel phase. The crystallite sizes (or coherent diffraction domain size) and lattice parameters are given in Table 1. To compare, we report the values of Fe_3O_4 and γ-Fe_2O_3 taken from the JCPDS files no. 19-0629 and no. 39-1346. The lattice parameters of the Fe0.3 and Fe0.8 samples are very similar to those of magnetite, so after an initial observation, these compounds could be described as being similar to stoichiometric magnetite (we will see later in the text that having considered the Mössbauer results, it is not the case). On the contrary, the Fe0.1 sample has a lower lattice parameter and can thus be identified as nonstoichiometric. Assuming that the variation of the lattice parameters between Fe_3O_4 and γ-Fe_2O_3 is linear [16], the approximate stoichiometry of Fe0.1 is $Fe_{2.87}O_4$.

The size and morphology of the powders are examined by scanning electron microscopy (SEM). Fig. 2 shows representative images of the Fe0.1, Fe0.3 and Fe0.8 samples. It can be seen that Fe0.1 and Fe0.3 are very similar, being constituted of sub-micrometric spheres with a diameter equal to (146 ± 40) nm and (230 ± 61) nm respectively. For the both two samples, each micro-sphere contains many crystallites. The mean size of crystallites (determined from 50 crystallites) is slightly lower for Fe0.1 than for Fe0.3, being (30 ± 6) nm and (44 ± 10) nm respectively. These values are coherent with those determined by XRD. For Fe0.8, the powder morphology is very different. It appears as compact and faceted particles with a size between approximately 100 and 150 nm. As the crystallite size (determined by XRD) is similar to the particle size, it can be concluded that the Fe0.8 particles are monocrystalline. However, it appears that some particles are aggregated.

In order to determine the stoichiometry of the compound, Mössbauer spectrometry is performed at room temperature. At 300 K, the Mössbauer spectrum of stoichiometric magnetite can be described by two magnetic components. The outer sextet (denoted M1) is attributed to Fe^{3+} ions in A sites and the inner sextet (denoted M2) is attributed to Fe^{3+} and Fe^{2+} ions in B sites. At this temperature, the electron exchange between Fe(II) and Fe(III) is faster than the Larmor precession, so the parameters of the inner sextet are characteristic of an intermediate state between Fe^{3+} and Fe^{2+} (see parameters in Table 2) [17,18].

Fig. 3 shows the Mössbauer spectra of Fe0.1, Fe0.3 and Fe0.8 samples. Each spectrum is composed of two magnetic components. As the lines of the M2 contribution are noticeably wider than the lines of the M1 contribution, each spectrum is fitted according to the following method: the outer magnetic lines are fitted with one sextet and the inner magnetic contribution is fitted with a distribution of hyperfine fields. Each sub-spectrum of the distribution is assumed to have the same isomer shift and quadrupolar shift. The hyperfine parameters obtained and area ratio between M1 and M2 contributions are given in Table 2. In natural magnetite, the area ratio is 1:1.93 (not exactly 1:2 as expected because of the different recoilless fractions for the two sites [18,19]). In our samples, the area ratio is very different from that observed in stoichiometric magnetite, in particular for the Fe0.1 sample. So, it can be concluded, that our samples are not composed of stoichiometric magnetite but of nonstoichiometric magnetite. In this case, M1 and M2 contributions must be interpreted in a different way. In nonstoichiometric magnetite, the Fe^{3+} ions in A site and in B site have similar hyperfine parameters. Thus, the M1 contribution is due to Fe^{3+} in A site and also to Fe^{3+} in B site (the M2 contribution remaining the same). So the inner and outer sextet relative surface area ratio is a good measurement of nonstoichiometry. The number of cation vacancies x in $Fe_{3-x}O_4$ is thus given by the relation: $x = \frac{2-S}{5S+6}$, S being the ratio between M2 and M1 areas [20].

The values obtained for x are reported in Table 2 (for the calculation, recoilless fractions of both iron ions were supposed to be identical). In agreement with XRD results, it can be seem that the vacancy content is very similar for the Fe0.3 or Fe0.8 samples, and lower than for the Fe0.1 sample. The slight difference between the values determined by XRD and Mössbauer spectroscopy is attributed to the fact that the recoilless fractions are not exactly the same for the iron ions in A and B sites.

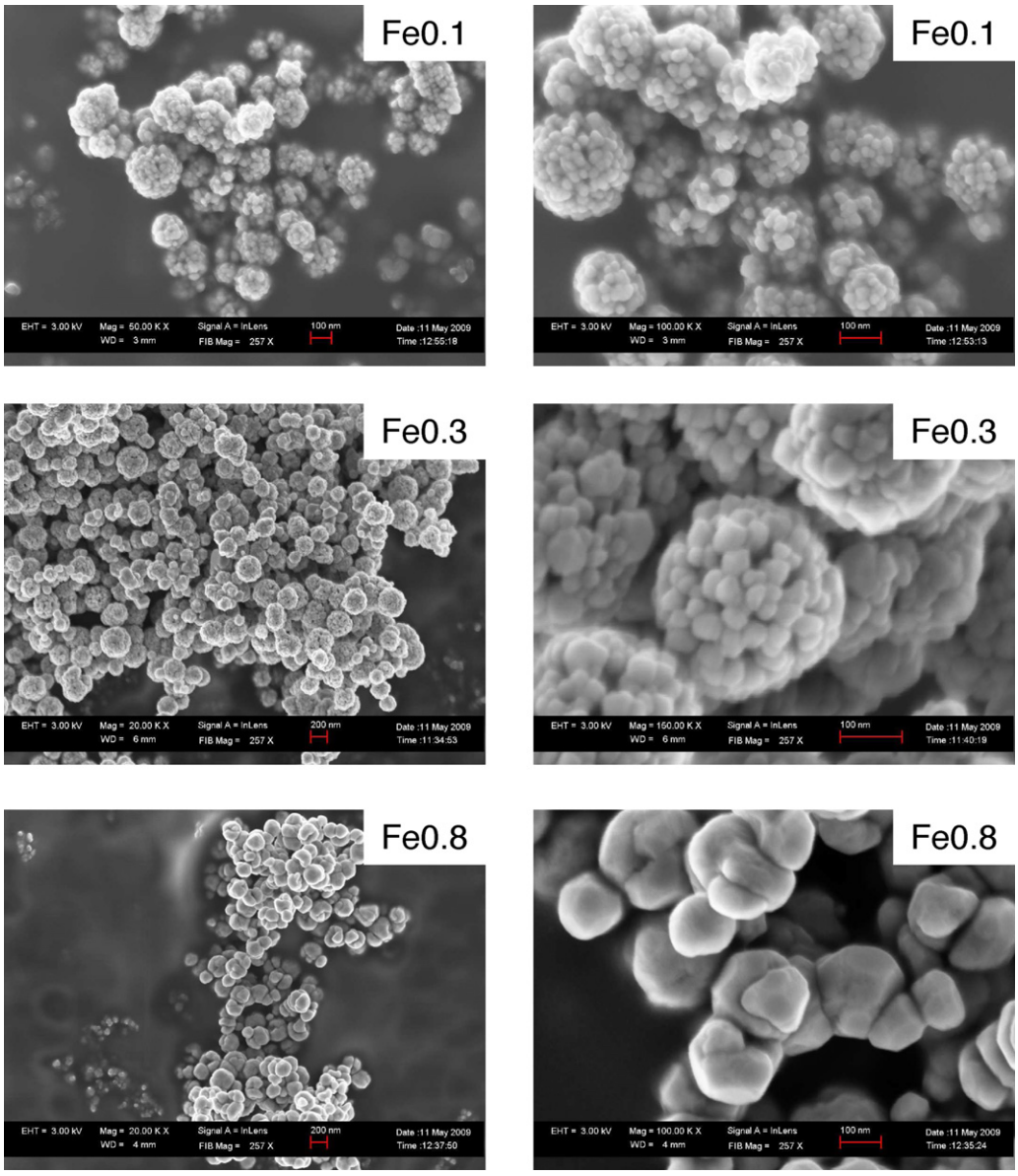

Fig. 2. SEM images of Fe0.1, Fe0.3 and Fe0.8 powders.

All these results show that the molar concentration of Fe^{3+} ions is a very important parameter that controls both the morphology and the crystallite size of the magnetite phase. Concentrations of 0.13 and 0.28 mol L^{-1} lead to the same particle shape (microspheres composed of many crystallites) but do not lead to the same stoichiometry ($Fe_{2.79}O_4$ and $Fe_{2.92}O_4$ respectively). The difference in stoichiometry can be explained by a partial oxidation of the samples during the drying stage at 60 °C. Indeed, the magnetite is easily

Table 2
^{57}Fe hyperfine parameters obtained at room temperature of Fe0.1, Fe0.3 and Fe0.8 samples and Fe_3O_4.

Sample	Assignation	δ[a] (mm s^{-1})	Γ (mm s^{-1})	2ε (mm s^{-1})	B[b] or $B_{average}$ (T)	Area ratio	Stoichiometry
Fe0.1	M1	0.33	0.55	−0.07	49.0	1	$Fe_{2.79}O_4$
	M2	0.49	–	−0.09	43.5	0.36	
Fe0.3	M1	0.28	0.44	−0.07	48.3	1	$Fe_{2.92(2)}O_4$
	M2	0.67	–	−0.04	45.4	1.10	
Fe0.8	M1	0.30	0.42	−0.06	48.7	1	$Fe_{2.91(8)}O_4$
	M2	0.67	–	−0.08	45.4	1.07	
Natural magnetite[c]	M1	0.26	–	−0.02	49.0	1	Fe_3O_4
	M2	0.67	–	0.00	46.0	1.93	

M1 and M2 correspond to the outer and inner sextets, respectively. Estimated errors for δ, Γ, 2ε, B and area ratio are ±0.01 mm s^{-1}, 0.01 mm s^{-1}, 0.01 mm s^{-1}, 0.5 T and 0.05 respectively.

[a] Relative to metallic iron.

[b] B is the hyperfine field of the outer sextet and $B_{average}$ is the average hyperfine field corresponding to the inner sextet.

[c] Natural magnetite from [13].

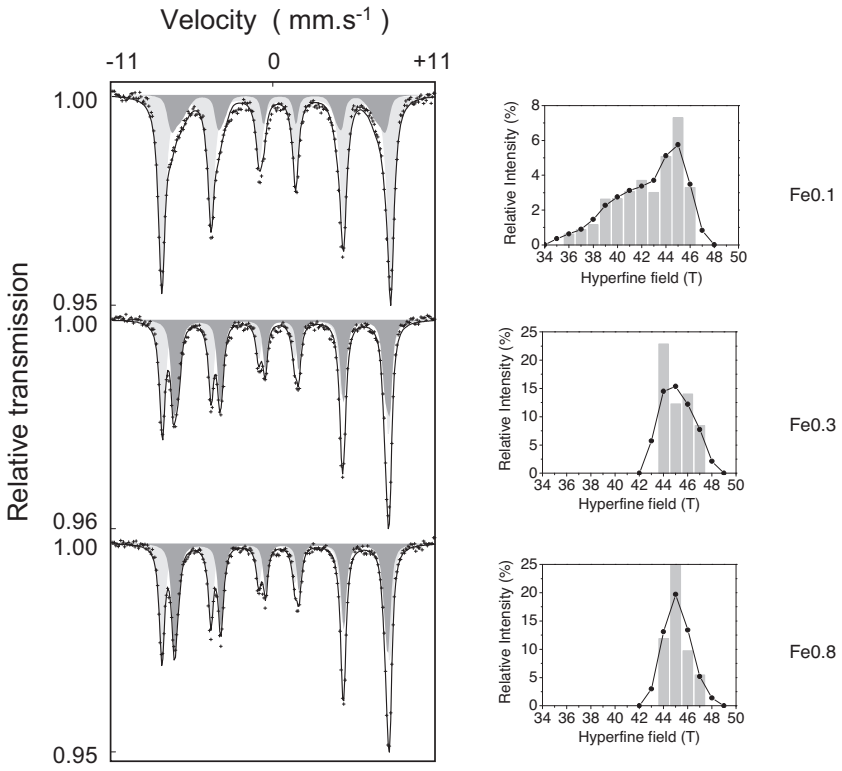

Fig. 3. (left): Mössbauer spectra of Fe0.1, Fe0.3 and Fe0.8 samples. (right): hyperfine field distributions corresponding to the inner sextet (bars: experimental values, points and curve: average values determined by $I_{average} = (I_{n-1} + 2I_n + I_{n+1})/4$.

oxidized and transforms in to maghemite at a low temperature air. The transformation kinetics increases strongly when the crystallite size decreases [9]. So as the crystallite size of the Fe0.1 sample is lower than that of Fe0.3 sample, Fe0.1 is more oxidized. Even if the particles do not have the same morphology, for a concentration of 0.78 mol L^{-1} and 0.28 mol L^{-1}, the stoichiometry of magnetite is almost the same. This is probably due to the fact that beyond a critical crystallite size, the magnetite rate of oxidation is similar.

When CH_3CO_2Na is added to the iron solution, we observe the formation of a pale brown precipitate and a strong smell of acetic acid. Then, the aging at 200 °C for 21 h lead to the formation of magnetite. So the possible reaction process can be described as follows:

(i) Formation of iron hydroxide: $Fe^{3+} + 3CH_3CO_2Na + 3H_2O \rightarrow 3CH_3CO_2H + Fe(OH)_3$
(ii) Reduction of $Fe(OH)_3$ to Fe_3O_4 by ethylene glycol: $Fe(OH)_3 \rightarrow Fe_3O_4$

The reaction (i) demonstrates that sodium acetate plays an important role in the magnetite formation. When the ratio between acetate ions and iron ions is lower than 3, the powder obtained is a mixture of Fe_2O_3 and Fe_3O_4. These results are in agreement with those of Yan et al. [21].

Microspheres composed of many single crystallites (so-called colloidal nanocrystal clusters) have been already observed with different kinds of ferrites, such as 100–200 nm manganese–zinc ferrite [22], 100–200 nm nickel ferrite [23] or 200–300 nm magnetite [12]. For Ge et al. [24] who also synthesized magnetite using the solvothermal method, the formation of the nanocrystal cluster occurs in two steps: primary nanocrystals nucleate in a supersaturated solution and then aggregate into larger secondary particles to minimize the surface energy. This mechanism can explain the particle formation obtained for low iron concentrations, but it is different for higher concentrations. Indeed the particles obtained are compact more or less agglomerated microspheres. In this case, after the initial nucleation stage, the crystal nuclei do not agglomerate but grow, leading on to the formation of micro-particles. This mechanism difference is probably due to the difference in water concentration. As the iron III chloride is hexahydrated, when the iron concentration increases a water content increase too. The latter varies from 1 to 8 percent between the Fe0.1 sample and Fe0.8 sample. Wang et al. [25] and Cho et al. [26] have shown that the morphology of Fe_3O_4 particles obtained via a solvothermal route can be controlled by the water content. In particular, the particle size increases when the amount of water increases. To sum up, the Fe_3O_4 particle morphology changes with the ethylene glycol/water ratio.

3.2. Magnetic properties

The magnetic properties of the samples are investigated with a SQUID magnetometer at room temperature (300 K) and at 5 K (see Fig. 4). The hysteresis loops are very similar, all the samples are rapidly saturated. The specific saturation magnetization (σ_S) and the coercivity (H_c) are reported in Table 3.

The specific saturation magnetization of the Fe0.1 sample is lower than that of the other samples. This is due to the fact that Fe0.1 sample is strongly oxidized. It has been proven that, σ_S decreases when the number of vacancies (x) increases [13]. The saturation magnetization of the Fe0.3 sample is found to be lower than that of the Fe0.8 sample although both samples have the same stoichiometry. But they do not have the same crystallite size (43 and 121 nm respectively). This phenomenon has been observed in different ferrites and is explained by the existence of a magnetically dead layer on the particle surface [3], the saturation magnetization thus decreases with the crystallite size. For all the samples, the values of σ_S at 300 K are lower than those at 5 K. The reason for this is

Table 3
Specific saturation magnetization and coercive field determined at 5 and 300 K for Fe0.1, Fe0.3 and Fe0.8 samples.

Sample	σ_S* at 5 K (emu/g)	σ_S* at 300 K (emu/g)	H_c at 5 K (Oe)	H_c at 300 K (Oe)
Fe0.1	87	77	290	49
Fe0.3	89	81	223	43
Fe0.8	98	89	215	52

Estimated errors for σ_S and H_c are 2 emu/g and 5 Oe respectively (the error were estimated by measuring 3 times a similar sample).
*Values determined at 5 T.

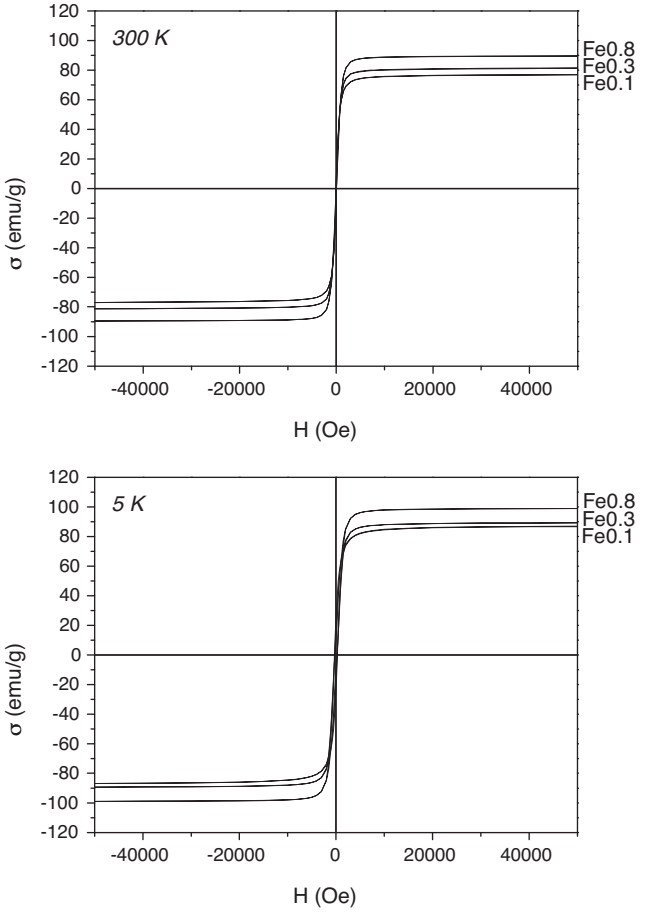

Fig. 4. Hysteresis loops measured at 5 K and 300 K for Fe.01, Fe0.3 and Fe0.8 samples.

that the thermal energy above 0 K causes some misalignment of the magnetic moments. Generally, the evolution of magnetization can be described by a spin-wave type dependence: $M_s = M_0(1 - a\,T^{2/3})$ where M_s, M_0, and a are respectively the saturation magnetization at the temperature T, the saturation magnetization at 0 K and the Bloch constant. The values of the coercive field are similar to those usually observed for magnetite or nonstoichiometric magnetite [3].

4. Conclusions

To sum up, nonstoichiometric magnetite particles are synthesized via a polyol process using ethylene glycol as the solvent and reducing agent. The influence of the concentration of Fe^{3+} ions on both size and morphology of the obtained particles is investigated. Our results show that for 0.1 and 0.3 mol L^{-1} concentrations, the particles are constituted of sub-micrometric spheres and each micro-sphere contains many crystallites, the crystallite size increasing in correlation with the iron concentration. XRD and Mössbauer spectrometry show that the samples are more oxidized when the crystallite size is small. For a 0.8 mol L^{-1} concentration, the magnetite particle are quasi-monocrystalline compact spheres with a diameter between approximately 100 and 250 nm. The initial concentration of iron is therefore an important parameter which governs the morphology and the properties of the magnetite particles. However, the coercive field values of and the values of the saturation magnetization are the same as those usually obtained.

Acknowledgments

The authors thank Mrs. Laurence Chevalier and Mr. Jean-Jacques Malandain for SEM investigations.

References

[1] P.I. Girginova, A.L. Daniel-da-Silva, C.B. Lopes, P. Figueira, M. Otero, V.S. Amaral, E. Pereira, T. Trindade, J. Colloid Interface Sci. 345 (2010) 234–240.
[2] X.S. Wang, L. Zhu, H.J. Lu, Desalination 276 (2011) 154–160.
[3] J. Mürbe, A. Rechtenbach, J. Töpfer, Mater. Chem. Phys. 110 (2008) 426–433.
[4] C. Sun, J.S.H. Lee, M. Zhang, Adv. Drug Deliv. Rev. 60 (2008) 1252–1265.
[5] S. Laurent, S. Dutz, U.O. Häfeli, M. Mahmoudi, Adv. Colloid Interface Sci. 166 (2011) 8–23.
[6] J.P. Déry, E.F. Borra, A.M. Ritcey, Chem. Mater. 20 (2008) 6420–6426.
[7] S. Ni, D. He, X. Yang, T. Li, J. Alloys Compd. 509 (2011) L305–L307.
[8] T. Iwasaki, N. Sato, K. Kosaka, S. Watano, T. Yanagida, T. Kawai, J. Alloys Compd. 509 (2011) L34–L37.
[9] K. Haneda, A.H. Morrish, J. Phys. Paris 38 (1977) C1321–C1323.
[10] P. Hu, S. Zhang, H. Wang, D. Pan, J. Tian, Z. Tang, A.A. Volinsky, J. Alloys Compd. 509 (2011) 2316–2319.
[11] S. Asuha, B. Suyala, X. Siqintana, S. Zhao, J. Alloys Compd. 509 (2011) 2870–2873.
[12] X. Liu, S. Fu, H.-M. Xiao, J. Solid State Chem. 179 (2006) 1554–1558.
[13] R.M. Cornell, U. Schwertmann, The Iron Oxides. Structure, Properties, Reactions, Occurrence and Uses, VCH Verlagsgesellschaft, Weinheim, 1996.
[14] E.J.W. Verwey, E.L. Heilmann, J. Chem. Phys. 15 (1947) 174–180.
[15] J.I. Langford, NIST Spec. Publ. 846 (1992) 110–126.
[16] E. Schmidbauer, M. Keller, J. Magn. Magn. Mater. 297 (2006) 107–117.
[17] R. Bauminger, S.G. Cohen, S. Ofer, E. Segal, Phys. Rev. 122 (1961) 1447–1450.
[18] G.J. Long, Mössbauer Spectroscopy Applied to Inorganic Chemistry, Plenum Press, New York and London, 1987.
[19] G.A. Sawatzky, F. Van der Woude, A.H. Morrish, Phys. Rev. 183 (1969) 383–386.
[20] H. Topsoe, J.A. Dumesic, M. Boudart, J. Phys. Paris 12 (1974) C6411–C6413.
[21] H. Yan, Z. Liping, H. Weivei, L. Xiaojuan, L. Xiangnong, Y. Yuxiang, Glass Phys. Chem. 36 (2010) 325–331.
[22] Q. Zhang, M. Zhu, Q. Zhang, Y. Li, H. Wang, J. Magn. Magn. Mater. 321 (2009) 291–294.
[23] J. Wang, F. Ren, R. Yi, A. Yan, G. Qiu, X. Liu, J. Alloys Compd. 479 (2009) 791–796.
[24] J. Ge, Y. Hu, M. Biasini, W. Beyermann, Y. Yin, Angew. Chem. Ger. Ed. 46 (2007) 4342–4345.
[25] X. Wang, Z. Zhao, J. Qu, Z. Wang, J. Qiu, Cryst. Growth Des. 10 (2010) 2863–2869.
[26] S.B. Cho, J.S. Noh, S.J. Park, D.Y. Lim, S.H. Choi, J. Mater. Sci. 42 (2007) 4877–4886.